Available online at www.sciencedirect.com
SCIENCE DIRECT®
Journal of Computational Physics 211 (2006) 424–447
JOURNAL OF COMPUTATIONAL PHYSICS
www.elsevier.com/locate/jcp

Simple derivation of high-resolution schemes for compressible flows by kinetic approach

Taku Ohwada *, Satoshi Fukata

Department of Aeronautics and Astronautics, Graduate School of Engineering, Kyoto University, Sakyo-ku, Kyoto 606-8501, Japan

Received 14 October 2004; received in revised form 8 March 2005; accepted 15 April 2005
Available online 20 July 2005

Abstract

The high-resolution scheme for the compressible Navier–Stokes equations developed in Ohwada and Kobayashi [Management of discontinuous reconstruction in kinetic schemes, J. Comput. Phys. 197 (2004) 116–138] is rederived without using any special techniques of kinetic theory. The scheme is simplified and its efficiency is improved by introducing an artificial equilibrium function. High performance of the new scheme is demonstrated in the problems of double-Mach-reflection, forward-facing step, and shock-boundary-layer interaction. The detailed information for easy programming is also given.

PACS: 65M06; 65M25; 65M15; 76P05; 76N10

Keywords: High-resolution scheme; Kinetic scheme; Euler equations; Navier–Stokes equations

1. Introduction

The performance of home computer was improved drastically in the last two decades. In fact, a recent home computer can easily do the same large-scale fluid-dynamic computation as was carried out on a super computer in a research institute 20 years ago, even while performing a web-browsing program. Although the resources of ''super computing'' are now widely prevailing, never does it mean that the computational fluid dynamics (CFD) became easily accessible in these 20 years, however.

The high-resolution scheme for capturing shock waves and contact discontinuities is not regarded as an appropriate topic for undergraduate students at the present time. It is now provided as one of the advanced

* Corresponding author. Tel.: +81 75 753 5801; fax: +81 75 753 4947.
E-mail address: ohwada@kuaero.kyoto-u.ac.jp (T. Ohwada).

0021-9991/$ - see front matter
doi:10.1016/j.jcp.2005.04.026

topics for graduate students or professionals in the field of aerospace engineering and its related areas. This situation is mainly due to the depth of theory of approximate Riemann solver (see, e.g. [11]), which is prerequisite for the clear understanding of most of high-resolution schemes. In kinetic approach to compressible flows, such as the equilibrium flux method (EFM) [10], the kinetic flux vector splitting scheme (KFVS) [1], and the gas kinetic BGK scheme (GKB) [15], this cumbersome task even for professionals is bypassed; the linearity of the convective term in the kinetic equation drastically simplifies the theory of characteristics. One may think that this seemingly easy job should be compensated with the additional task of learning advanced knowledge of kinetic theory. In fact, the EFM and KFVS can be regarded as the deterministic variants of the direct simulation Monte-Carlo (DSMC) of the Boltzmann equation for the case of vanishing mean free path and the KFVS and GKB for the compressible Navier–Stokes equations employ the second order approximation in the Chapman–Enskog expansion. In other words, the clear understanding of kinetic approach seems to require the knowledge of asymptotic analysis and numerical analysis of kinetic equations. However, the past studies on kinetic schemes, e.g. [6,8,9], imply that the derivation of kinetic schemes for gas-dynamic equations up to the Navier–Stokes order does not require any advanced knowledge of kinetic theory.

In [7], a kinetic scheme for the compressible Navier–Stokes equations, which is shock capturing and yields a fine boundary-layer profile under a reasonable resolution, is developed. Since some techniques of kinetic theory, such as the Chapman–Enskog expansion and the splitting algorithm for the Boltzmann equation, are employed in the derivation, it is not readily accessible to the engineering community at large. The objective of the present paper is to show that such high-resolution schemes are derived without using any advanced knowledge of gas-dynamics including kinetic theory. We summarize the outcome of the recent studies on kinetic schemes [7,8] as the simple derivation of high-resolution schemes for compressible flows and demonstrate the high performance.

The organization of the paper is as follows. In Section 2, the principle of kinetic scheme is reviewed in the framework of the approximate method for the one-dimensional compressible Euler equations. In Section 3, a high-resolution scheme is derived as a hybrid between two kinetic schemes employing different reconstructions of fluid-dynamic variables. Section 4 is devoted to the extension and generalization of the scheme. The hybrid scheme is extended to the case of the compressible Navier–Stokes equations and to the case of polyatomic gases. The scheme in [7] employs the real equilibrium function, i.e., the local Maxwellian. The generalization of the equilibrium function is also discussed there. The numerical results are presented in Section 5, where the double-Mach-reflection, forward-facing step, and shock-boundary-layer interaction, which are typical 2D test cases in CFD, are solved with high accuracy and high efficiency. The detailed information of the scheme for easy programming is also presented in Appendix A.

2. Principle of kinetic scheme

We review the principle of kinetic schemes for compressible flows. For the brief explanation, we consider the one-dimensional Euler equations for ideal gases:

$$\frac{\partial \boldsymbol{h}}{\partial t} + \frac{\partial \boldsymbol{\Phi}(\boldsymbol{h})}{\partial x_1} = 0, \tag{1}$$

$$\boldsymbol{h} = (\rho, \rho u_i, \rho[e + u_k^2/2])^{\mathrm{T}}, \tag{2}$$

$$\boldsymbol{\Phi} = (\rho u_1, \rho u_1 u_i + p\delta_{1i}, \rho u_1[e + u_k^2/2] + p u_1)^{\mathrm{T}}, \tag{3}$$

where x_1 is the space coordinate and t is the time; ρ, u_i, p, and e are the density, flow velocity, pressure, and internal energy (per unit mass) of the gas, respectively; δ_{ij} is Kronecker's delta; u_k^2 means $u_1^2 + u_2^2 + u_3^2$ (Einstein's summation convention); and the superscript T means the transpose. For ideal gases, $p = R\rho T$ and

$e = C_v T$, where T is the temperature of the gas, R is the specific gas constant, and C_v is the isochoric specific heat, i.e., $C_v = (3 + K)R/2$ for K internal degrees of freedom.

2.1. Finite volume method

Many of the existing high-resolution schemes for compressible flows are categorized into the finite volume method. In this approach for the one-dimensional case, the space region, x_1, is divided into cells. Let the domain of ith cell be the interval $(x^{i-1/2}, x^{i+1/2})$ $(i = 1, 2, 3, \ldots)$. Integrating both sides of Eq. (1) over the cell $(x^{i-1/2}, x^{i+1/2})$ and the time interval $(0, \Delta t)$, we have

$$\boldsymbol{h}^i(\Delta t) = \boldsymbol{h}^i(0) - \frac{1}{\Delta x}[\boldsymbol{F}^{i+1/2} - \boldsymbol{F}^{i-1/2}], \tag{4}$$

where $\Delta x = x^{i+1/2} - x^{i-1/2}$, $\boldsymbol{h}^i(t)$ is the average of $\boldsymbol{h}(x_1, t)$ over the ith cell, i.e.,

$$\boldsymbol{h}^i(t) = \frac{1}{\Delta x}\int_{x^{i-1/2}}^{x^{i+1/2}} \boldsymbol{h}(x_1, t)\, \mathrm{d}x_1, \tag{5}$$

and $\boldsymbol{F}^{i+1/2}$ is the numerical flux at $x_1 = x^{i+1/2}$ defined by

$$\boldsymbol{F}^{i+1/2} = \int_0^{\Delta t} \boldsymbol{\Phi}[\boldsymbol{h}(x^{i+1/2}, t)]\, \mathrm{d}t. \tag{6}$$

We will show three different derivations of the same formula of the numerical flux, which is second order accurate in time.

2.2. Cauchy–Kowalevskaya procedure for analytic initial data

Evaluating the time derivative of the flux function $\boldsymbol{\Phi}$ in Eq. (6) by using Eq. (1) (Cauchy–Kowalevskaya procedure), we have the following formula with the second order accuracy in time:

$$F_k^{i+1/2} = \Delta t \Phi_k - \frac{\Delta t^2}{2}\frac{\partial \Phi_k}{\partial h_j}\frac{\partial \Phi_j}{\partial h_m}\frac{\partial h_m}{\partial x_1}, \tag{7}$$

where each term on the right hand side is evaluated at $(x_1, t) = (x^{i+1/2}, 0)$, the subscripts j, k, and m mean the components of vectors, and Einstein's summation convention is employed.

2.3. Cauchy–Kowalevskaya procedure at microscopic level

We will derive Eq. (7) by a kinetic method. Here, for simplicity, we consider the case of monatomic gases $(K = 0)$. We first summarize the minimum knowledge of kinetic theory which is necessary for this job.

(i) *kinetic definition of fluid-dynamic variables.* The fluid-dynamic variables are defined by the moments of the distribution function of the gas molecules f, which is a function of x_1, t, and the molecular velocity $\boldsymbol{\xi}$, i.e., $f(x_1, t, \boldsymbol{\xi})$. The conservative variables $\boldsymbol{h}$ are given by

$$\boldsymbol{h} = \int \boldsymbol{\psi} f\, \mathrm{d}\boldsymbol{\xi}, \tag{8}$$

where the vector $\boldsymbol{\psi}$ is defined by $\boldsymbol{\psi} = (1, \xi_i, \xi_k^2/2)^{\mathrm{T}}$ and the domain of the integration is the whole velocity space R^3 (this is applied to all the following integrals with respect to $\boldsymbol{\xi}$, unless otherwise stated); the primitive variables $\tilde{\boldsymbol{h}} = (\rho, u_i, T)^{\mathrm{T}}$ are obtained from $\boldsymbol{h}$.

(ii) *Equilibrium function.* A local equilibrium state of the gas is described by the local Maxwellian, which depends on x_1 and t through the macroscopic parameters $\boldsymbol{h}$ (or $\tilde{\boldsymbol{h}}$), i.e., $g[\boldsymbol{h}(x_1,t),\boldsymbol{\xi}]$ or $g[\tilde{\boldsymbol{h}}(x_1,t),\boldsymbol{\xi}]$, and its functional form with respect to $\boldsymbol{\xi}$ is given by

$$g = \frac{\rho}{(2\pi RT)^{3/2}} \exp\left[-\frac{(\xi_i - u_i)^2}{2RT}\right]. \tag{9}$$

The local Maxwellian g satisfies

$$\boldsymbol{h} = \int \boldsymbol{\psi} g \, \mathrm{d}\boldsymbol{\xi} \tag{10}$$

and yields the flux function for the compressible Euler equations $\boldsymbol{\Phi}$

$$\boldsymbol{\Phi} = \int \xi_1 \boldsymbol{\psi} g \, \mathrm{d}\boldsymbol{\xi}, \tag{11}$$

where ξ_1 is the component of molecular velocity in the direction of x_1, which is normal to the cell interface. Hereafter, we call the function $g[\boldsymbol{h}(x_1,t),\boldsymbol{\xi}]$ the equilibrium function if it satisfies Eqs. (10) and (11). We will explain the derivation of kinetic schemes using the properties of the equilibrium function, Eqs. (10) and (11); the explicit functional form of the equilibrium function will not be used until the final stage (the last part of Appendix A). The above gadgets are for the case of monatomic gases and those for polyatomic gases will be summarized in Section 4.

Inserting Eq. (11) into Eq. (6), expanding g in the integrand around $t = 0$, and making use of Eq. (1) for the evaluation of $\partial g/\partial t$, we have the formula of the numerical flux:

$$\boldsymbol{F}^{i+1/2} = \int_0^{\Delta t} \int \xi_1 \boldsymbol{\psi} f(x^{i+1/2}, t, \boldsymbol{\xi}) \, \mathrm{d}\boldsymbol{\xi} \, \mathrm{d}t, \tag{12}$$

$$f(x^{i+1/2}, t, \boldsymbol{\xi}) = g - t\frac{\partial g}{\partial h_k}\frac{\partial \Phi_k}{\partial x_1} = g - t\frac{\partial g}{\partial h_k}\frac{\partial \Phi_k}{\partial h_m}\frac{\partial h_m}{\partial x_1} = g - t\frac{\partial g}{\partial h_k}\left(\int \xi_1 \psi_k \frac{\partial g}{\partial h_m} \, \mathrm{d}\boldsymbol{\xi}\right)\frac{\partial h_m}{\partial x_1}, \tag{13}$$

where each term on the right hand side is evaluated at $(x_1,t) = (x^{i+1/2},0)$. It is easily verified that $\boldsymbol{F}^{i+1/2}$ defined by Eqs. (12) and (13) is equivalent to Eq. (7). Eq. (13) will be employed as the canonical solution in the kinetic construction of high-resolution schemes, which are second order accurate in time. We have considered the conservative variables $\boldsymbol{h}$ as the arguments of the equilibrium function. The primitive variables $\tilde{\boldsymbol{h}}$ can also be employed as its macroscopic parameters; Eqs. (7) and (13) are rewritten as:

$$F_k^{i+1/2} = \Delta t \Phi_k - \frac{\Delta t^2}{2}\frac{\partial \Phi_k}{\partial h_j}\frac{\partial \Phi_j}{\partial \tilde{h}_m}\frac{\partial \tilde{h}_m}{\partial x_1}, \tag{14}$$

$$f(x^{i+1/2}, t, \boldsymbol{\xi}) = g - t\frac{\partial g}{\partial h_k}\frac{\partial \Phi_k}{\partial \tilde{h}_m}\frac{\partial \tilde{h}_m}{\partial x_1} = g - t\frac{\partial g}{\partial h_k}\left(\int \xi_1 \psi_k \frac{\partial g}{\partial \tilde{h}_m} \, \mathrm{d}\boldsymbol{\xi}\right)\frac{\partial \tilde{h}_m}{\partial x_1}. \tag{15}$$

2.4. Railroad method

In this section, we briefly explain a more complete theory for the construction of kinetic schemes, which is called the railroad method [5–7]. The reader who is interested only in the explicit construction of the kinetic scheme can safely skip to Section 3.

In the previous subsection, we derived Eqs. (12) and (13) [and consequently Eq. (7)] by considering the equilibrium function, the local Maxwellian, the macroscopic parameters of which satisfy Eq. (1). It

is easily verified by the direct substitution that such a distribution function satisfies the following kinetic equation:

$$\frac{\partial f}{\partial t} + \xi_1 \frac{\partial f}{\partial x_1} = -\frac{\partial g}{\partial h_k}\frac{\partial \Phi_k}{\partial x_1} + \xi_1 \frac{\partial g}{\partial x_1}, \tag{16}$$

where the argument $\boldsymbol{h}$ (or $\tilde{\boldsymbol{h}}$) of each term on the right hand side is defined by Eq. (8). Multiplying Eq. (16) by $\boldsymbol{\psi}$ and integrating the results over the whole velocity space, the cell $(x^{i-1/2},x^{i+1/2})$, and the time interval $(0,\Delta t)$, we have Eq. (4) with Eq. (12). The right hand side of Eq. (16) vanishes after the integration with respect to $\boldsymbol{\xi}$, since $\int \psi_k(\partial g/\partial h_j)\,\mathrm{d}\boldsymbol{\xi} = \delta_{jk}$ and $\int \psi_k \xi_1(\partial g/\partial x_1)\,\mathrm{d}\boldsymbol{\xi} = \partial \Phi_k/\partial x_1$. In this formulation, we consider the Cauchy problem of Eq. (16) from the initial data in the form of $f = g$. Consequently, the distribution function f in Eq. (12) should be the solution of the Cauchy problem. The solution is formally expressed as the sum of the term corresponding to the initial data and the integration of the collision term, the right hand side of Eq. (16), along the characteristics $x_1(s) = x^{i+1/2} - \xi_1(t-s)$. Applying the Euler method to the integral along the characteristics and using the Taylor expansion around $(x_1,t) = (x^{i+1/2},0)$, we have the canonical solution (13) as an approximate solution with the error of $\mathrm{O}(t^2)$.

2.5. Remarks

We have considered three derivations of Eq. (7). From the last two derivations, we obtained the canonical solution for the kinetic schemes with the second order accuracy in time. From the last (third) derivation, we got the principle of the extension to the case of the discontinuous reconstruction of the fluid-dynamic variables, i.e., the theory of characteristics of kinetic equation. Incidentally, the last derivation reveals the intrinsic error of the existing kinetic schemes. The contribution of the collision term of Eq. (16) to the canonical solution is $\mathrm{O}(t)$, and therefore, that to the numerical flux is $\mathrm{O}(\Delta t^2)$, which shows that the kinetic schemes employing the solution of the Cauchy problem for the collisionless Boltzmann equation from the initial data in the form of $f = g$, such as EFM, are at most first order accurate in time. In [9], which inherits the strategy of [3], the second order accurate flux is derived from the solution of the collisionless Boltzmann equation by introducing a distortion in the initial data. The distortion is determined in such a way that the resulting formula of the numerical flux agrees with Eq. (7). Contrastively, the second order accuracy is automatically gained in the above three derivations and the extension to the higher order accurate formulas (third order, fourth order, etc.) can be done straightforwardly. We refer the reader to [8], where the above three approaches are applied to the construction of high order accurate kinetic scheme for the Burnett equations.

3. High-resolution scheme

It is well-known that the Lax–Wendroff scheme produces spurious oscillations around shock waves and contact discontinuities. The Godunov scheme, which is the counterpart of the Lax–Wendroff scheme in the classic CFD, employs the piecewise constant reconstruction, i.e., $\boldsymbol{h}(x_1,0) = \boldsymbol{h}^i$ in $(x^{i-1/2},x^{i+1/2})$, and computes the numerical fluxes by means of Riemann solver. Owing to the numerical dissipation created by the discontinuities at cell interfaces, spurious oscillations are suppressed. However, the numerical dissipation is excessive and the numerical result is smeared even in resolved regions. Most of high-resolution schemes employ piecewise polynomials that allow discontinuities at cell interfaces, such as MUSCL and ENO, and the numerical fluxes are computed by means of Riemann solver. High-resolution is usually brought by cleverly avoiding the creation of maxima and minima in the reconstruction, which is interpreted as the control of the numerical dissipation via that of the discontinuities at cell interfaces. On the other hand, in the viscous computation of Blasius flow, the Lax–Wendroff scheme with the additive viscous

and heat conduction terms works quite well. Contrastively, the discontinuous reconstructions are not advantageous in this case. Although the numerical dissipation created by the discontinuous reconstruction is small under a reasonable resolution, however, it is not negligibly smaller than the physical viscosity, which is very small; the boundary-layer profile is considerably poisoned by the small numerical dissipation [15,7]. The continuous reconstruction is advantageous in the boundary-layer computation and disadvantageous in the shock-wave computation and vise versa for the discontinuous reconstruction. This "antinomy" should be resolved in the high-resolution scheme for the compressible NS equations.

3.1. Reconstruction of fluid-dynamic variables

Before proceeding to the construction of the scheme, we prepare three reconstructions of the fluid-dynamic variables. Recall that the domain of ith cell is the interval $(x^{i-1/2},x^{i+1/2})$. Let x^i be the center of gravity of ith cell, i.e., $x^i = (x^{i-1/2} + x^{i+1/2})/2$. Then, the first reconstruction, which will be called Reconstruction-I hereafter, is the line graph connecting $(x^i,\boldsymbol{h}^i)$ $(i = 1, 2, 3, \ldots)$. The second reconstruction, which will be called Reconstruction-II hereafter, is a piecewise linear interpolation that passes through $(x^i,\boldsymbol{h}^i)$ and allows a discontinuity at each cell interface $x_1 = x^{i+1/2}$. The slope of $\boldsymbol{h}$ (or that of $\tilde{\boldsymbol{h}}$) in each cell is computed by an appropriate slope limiter. In the present paper, the van Leer limiter [16] is employed. Then, at each cell interface $x_1 = x^{i+1/2}$, the reconstructed $\boldsymbol{h}(x_1,t = 0)$ has two limiting values, $\boldsymbol{h}(x^{i+1/2} \pm 0,t = 0)$. These reconstructions are schematically shown in Fig. 1 together with Reconstruction-III, which will be introduced in the following section.

3.2. Preliminary schemes

We employ the superscript 'I' to express the term approximated by Reconstruction-I. Applying Reconstruction-I to the canonical solution (13), we have

$$\begin{aligned} f(x^{i+1/2},t,\boldsymbol{\xi}) &= g^{\mathrm{I}} - t\left(\frac{\partial g}{\partial h_k}\frac{\partial \Phi_k}{\partial x_1}\right)^{\mathrm{I}} \\ &= g^{\mathrm{I}} - t\left(\frac{\partial g}{\partial h_k}\right)^{\mathrm{I}} \int \xi_1 \psi_k \left(\frac{\partial g}{\partial h_m}\frac{\partial h_m}{\partial x_1}\right)^{\mathrm{I}} \mathrm{d}\boldsymbol{\xi}, \end{aligned} \tag{17}$$

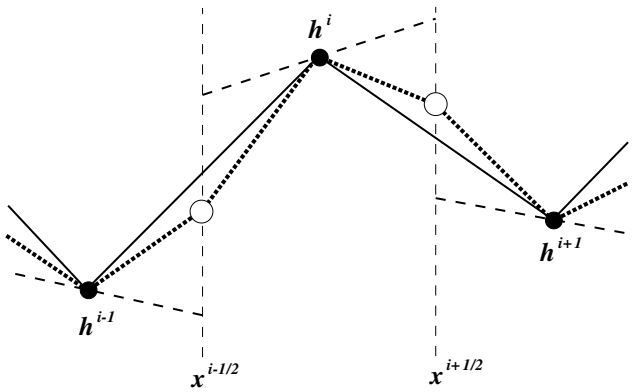

Fig. 1. The schematic figure of reconstruction: ———, Reconstruction-I; – – – –, Reconstruction-II; and ·····, Reconstruction-III (Section 3.2).

where each term on the right hand side is evaluated at $(x_1,t) = (x^{i+1/2},0)$. Substituting Eq. (17) into Eq. (12), we have the numerical flux of the Lax–Wendroff scheme. Therefore, the resulting scheme is not shock capturing and is excluded from the list of high-resolution schemes.

In the application of Reconstruction-II to the canonical solution (13), we take account of the direction of characteristics of the kinetic Eq. (16). We employ the superscript 'II' to express the term at $(x_1,t) = (x^{i+1/2},0)$ evaluated by this approximation, e.g.

$$g^{\mathrm{II}} = g(x^{i+1/2} \mp 0, 0, \boldsymbol{\xi}) \quad (\text{for } \xi_1 \gtrless 0). \tag{18}$$

Other terms in the canonical solution (13), i.e., $\partial g/\partial x_1$, $\partial g/\partial \boldsymbol{h}$, and $\partial h/\partial x_1$, are also approximated in the same way. Incidentally, Eq. (18) is interpreted physically; the molecules for $\xi_1 > 0$ come from the left hand side of the cell interface and those for $\xi_1 < 0$ comes from the right hand side. The explanation based on the physical intuition may be more understandable for the undergraduate students who are not familiar with kinetic theory. This is the reason why we said that Section 2.4 can be skipped, although a more complete theory than the Cauchy–Kowalevskaya procedure is presented there. As an extension of Eq. (13) to the case of Reconstruction-II, we have:

$$f(x^{i+1/2}, t, \boldsymbol{\xi}) = g^{\mathrm{II}} - t\left(\frac{\partial g}{\partial h_k}\right)^{\mathrm{II}} \Delta\Phi_k^{\mathrm{II}}, \tag{19}$$

$$\Delta\Phi_k^{\mathrm{II}} = \int \xi_1 \psi_k \left(\frac{\partial g}{\partial h_m}\frac{\partial h_m}{\partial x_1}\right)^{\mathrm{II}} \mathrm{d}\boldsymbol{\xi}. \tag{20}$$

The $\Delta\Phi_k^{\mathrm{II}}$ can also be computed by using the primitive variables $\tilde{\boldsymbol{h}} = {}^t(\rho, u_i, T)$:

$$\Delta\Phi_k^{\mathrm{II}} = \int \xi_1 \psi_k \left(\frac{\partial g}{\partial \tilde{h}_m}\frac{\partial \tilde{h}_m}{\partial x_1}\right)^{\mathrm{II}} \mathrm{d}\boldsymbol{\xi}. \tag{21}$$

Another formula for Reconstruction-II is

$$f = g^{\mathrm{II}} - t\left(\frac{\partial g}{\partial h_k}\frac{\partial \Phi_k}{\partial x_1}\right)^{\mathrm{II}}, \tag{22}$$

which yields Scheme-B for $\epsilon = 0$ of [7]. From these formulas, we have shock capturing schemes; the numerical flux is naturally split into two parts according to the sign of ξ_1, i.e., the direction of characteristics of Eq. (16). As mentioned before and shown in [7], the NS solver made by adding the viscous and heat conduction terms to the Euler solver for Reconstruction-II does not work in the boundary-layer computation because of the numerical dissipation created by the discontinuity.

The third reconstruction is a hybrid of Reconstruction-I and Reconstruction-II, which inherits the fine properties of the parents, i.e., its numerical dissipation becomes large in unresolved regions (Reconstruction-II), such as a shock layer, and small in resolved regions (Reconstruction-I), such as a boundary-layer. The hybridization is made at the microscopic level as follows. We first compute the value of $\boldsymbol{h}$ at each cell interface from g^{II}. We denote the result by $\boldsymbol{h}^{\mathrm{III}}$, i.e.,

$$\boldsymbol{h}^{\mathrm{III}} = \int \boldsymbol{\psi} g^{\mathrm{II}} \, \mathrm{d}\boldsymbol{\xi}. \tag{23}$$

Then, Reconstruction-III is made as the piecewise linear interpolation connecting $(x^i,\boldsymbol{h}^i)$ and $(x^{i+1/2},\boldsymbol{h}^{\mathrm{III}})$ $(i = 1, 2, 3, \ldots)$. The schematic figure of Reconstruction-III is shown in Fig. 1. Employing Reconstruction-III for g and $\partial g/\partial \boldsymbol{h}$ and Reconstruction-II for $\partial \boldsymbol{h}/\partial x_1$ in the canonical solution (13), we have

$$f(x^{i+1/2}, t, \boldsymbol{\xi}) = g^{\mathrm{III}} - t\left(\frac{\partial g}{\partial h_k}\right)^{\mathrm{III}} \Delta\Phi_k^{\mathrm{II}}, \tag{24}$$

where

$$g^{\mathrm{III}} = g(\boldsymbol{h}^{\mathrm{III}}, \boldsymbol{\xi}), \tag{25}$$

$$\left(\frac{\partial g}{\partial h_k}\right)^{\mathrm{III}} = \frac{\partial g}{\partial h_k}(\boldsymbol{h}^{\mathrm{III}}, \boldsymbol{\xi}). \tag{26}$$

The $\Delta\boldsymbol{\Phi}^{\mathrm{II}}$ remains as it is in Eq. (24) in order to link the time derivative of g and the numerical dissipation created by the discontinuity, which act in the opposite directions; the scheme becomes first order accurate in time when the slopes at both sides are reduced to zero by the limiter. If $\Delta\boldsymbol{\Phi}^{\mathrm{II}}$ is replaced by $\Delta\boldsymbol{\Phi}^{\mathrm{I}}$, spurious oscillations become remarkable. The scheme for Eq. (24) is equivalent to Scheme-F for $\epsilon = 0$ of [7]. It works well in the Blasius flow problem but it does not work very well in the Sod test case; small but appreciable spurious oscillations appear around the tail of the expansion wave. Although, this scheme works in the Sjögreen test case and the Woodward-Colella Blast-wave test case and considerable improvement over the Lax–Wendroff scheme is confirmed in several inviscid computations, it is excluded from the list of high-resolution schemes.

Incidentally, Reconstruction-III was devised by Xu in the construction of his GKB scheme [14,15]. The distribution function employed to compute the numerical flux of the GKB scheme is expressed as the integral form of the solution of Cauchy problem for the BGK equation, i.e., the sum of the term corresponding to the discontinuous initial data and the integral of the gain term (the local Maxwellian) along the characteristics. Reconstruction-III is employed in the approximation of the gain term. For $\tau \ll \Delta t$, the contribution of the gain term becomes dominant and Reconstruction-III plays the major role; the contribution of the initial data becomes dominant for $\Delta t \ll \tau$. Precisely speaking, however, the distribution function employed in the GKB scheme is not the approximate solution of the BGK equation for discontinuous initial data, since the Taylor expansion of the local Maxwellian around the singular point is employed formally in the derivation; the local Maxwellian created from the BGK solution for discontinuous initial data (Reconstruction-II) is singular around $(x_1,t) = (x^{i+1/2},0)$. Nevertheless, his construction is legitimated by the fact that the distribution function so constructed coincides with the canonical solution in the case of smooth initial data. Then, his construction of the BGK solution is interpreted as a procedure to mix Reconstruction-II and Reconstruction-III into the canonical solution. For the detailed analysis of the GKB scheme, we refer the reader to [7], where another way of mixing, which is based on the splitting algorithm, is proposed. In the following section, we will simply mix these reconstructions into the canonical solution without detouring to enjoy the above-mentioned techniques.

3.3. Hybridization

In Section 3.2, we made Reconstruction-III as the hybrid between Reconstruction-I and -II. For the successful high-resolution scheme, the hybridization at the level of numerical flux is necessary besides the hybridization at the level of reconstruction. In [7], a high-resolution scheme was developed as a hybrid between the scheme based on Eq. (22) and that based on Eq. (24). Since the weight factors employed there depend on t, the formula of the numerical flux is a little bit complicated. Here, we consider a simple hybridization. We apply the hybridization only to the equilibrium function g

$$f(x^{i+1/2}, t, \boldsymbol{\xi}) = \alpha g^{\mathrm{II}} + (1-\alpha) g^{\mathrm{III}} - t\left(\frac{\partial g}{\partial h_k}\right)^{\mathrm{III}} \Delta\Phi_k^{\mathrm{II}}, \tag{27}$$

where α is a positive constant and its value is determined at the beginning of each time step and for each cell interface. The principle of the hybridization is as follows. The value of the mixing parameter α is determined in such a way that the contribution of g^{II} becomes dominant in unresolved regions and small in resolved regions. So, various methods for the determination of α are considered. For example

$$\alpha = 1 - \exp\left[-C\frac{|h_k^+ - h_k^-|}{h_k^+ + h_k^-}\right], \tag{28}$$

where C is a positive constant, $h_k^\pm$ are the limiting values of h_k at the cell interface for Reconstruction-II. The value of C may depend on the position and time. A similar method is employed in the determination of τ of the GKB scheme [15]. Incidentally, the hybridization between Eqs. (17) and (19) does not work. The hybridization between the fortified Lax–Wendroff schemes by means of kinetic reconstructions is the key of the present kinetic scheme.

4. Extension

Up to now, we have considered the kinetic scheme of the compressible Euler equations for monatomic gases. In this section, we briefly explain the extensions to the cases of the compressible Navier–Stokes equations and polyatomic gases. We will also discuss the generalization of the equilibrium function.

4.1. Navier–Stokes equations

We have derived the kinetic scheme for the compressible Euler equations by using the local Maxwellian the macroscopic parameters of which satisfy the compressible Euler equations. The extension to the case of the compressible Navier–Stokes equations is done in the following way. We express the flux function for the compressible Navier–Stokes equations $\mathbf{\Phi}^{\mathrm{NS}}$ as the sum of the flux function for the compressible Euler equations $\mathbf{\Phi}$ and its correction (the diffusive flux) $\mathbf{\Phi}^1$, i.e.,

$$\mathbf{\Phi}^{\mathrm{NS}} = \mathbf{\Phi} + \mathbf{\Phi}^1. \tag{29}$$

Corresponding to the above expression, we express the distribution function that yields $\mathbf{\Phi}^{\mathrm{NS}}$ as the sum of the local Maxwellian and its correction f^1

$$f^{\mathrm{NS}} = g + f^1. \tag{30}$$

Then, f^{NS} should satisfy the relation

$$\mathbf{\Phi}^{\mathrm{NS}} = \int \xi_1 \boldsymbol{\psi} f^{\mathrm{NS}}\, \mathrm{d}\boldsymbol{\xi}. \tag{31}$$

From Eqs. (10) and (11), we notice that f^1 should satisfy:

$$\int \boldsymbol{\psi} f^1\, \mathrm{d}\boldsymbol{\xi} = 0, \tag{32}$$

$$\mathbf{\Phi}^1 = \int \xi_1 \boldsymbol{\psi} f^1\, \mathrm{d}\boldsymbol{\xi}. \tag{33}$$

In order to obtain the formula of the numerical flux, we expand f^{NS} around $t = 0$

$$f^{\mathrm{NS}}(x^{i+1/2}, t, \boldsymbol{\xi}) = g + f^1 + t\left(\frac{\partial g}{\partial t} + \frac{\partial f^1}{\partial t}\right) + \mathrm{O}(t^2), \tag{34}$$

where each term on the right hand side is evaluated at $(x_1,t) = (x^{i+1/2},0)$ and the time derivatives should be evaluated by using the compressible NS equations $\partial \boldsymbol{h}/\partial t + \partial \mathbf{\Phi}^{\mathrm{NS}}/\partial x_1 = 0$ in principle. Noting that the viscosity and thermal conductivity are proportional to the mean collision time of gas molecules τ, which is smaller than or of the same order of the time step Δt in the usual CFD computation, we simplify Eq. (34) by neglecting the terms of $\mathrm{O}(\tau t, t^2)$

$$f^{\mathrm{NS}}(x^{i+1/2}, t, \boldsymbol{\xi}) = g + f^{1} - t\frac{\partial g}{\partial h_k}\frac{\partial \Phi_k}{\partial x_1}. \tag{35}$$

Eq. (35) will be employed as the canonical solution for the compressible NS equations. Under the usual situation of CFD computation, i.e., $\tau \lesssim \Delta t$, Eq. (35) yields the effectively high order accurate numerical flux, the error of which is $O(\tau\Delta t^2, \Delta t^3)$; we can safely neglect $\partial f^1/\partial t$ and evaluate $\partial g/\partial t$ by using the compressible Euler equations. When f^1 is approximated by using Reconstruction-I, the extension of Eq. (27) to the case of the compressible NS equations is given by

$$f(x^{i+1/2}, t, \boldsymbol{\xi}) = \alpha g^{\mathrm{II}} + (1-\alpha) g^{\mathrm{III}} - t\left(\frac{\partial g}{\partial h_k}\right)^{\mathrm{III}} \Delta \boldsymbol{\Phi}_k^{\mathrm{II}} + (f^1)^{\mathrm{I}}. \tag{36}$$

In this extension, $(f^1)^{\mathrm{I}}$ becomes the central finite difference approximation of $\Delta t \boldsymbol{\Phi}^1$ in the formula of the numerical flux. Thus, the conventional extension of the Euler solver to the NS solver, i.e., the simple addition of the central finite difference approximation of the viscous and heat conduction terms, is recovered. Incidentally, in the case of the compressible NS equations derived from kinetic equations by the Chapman–Enskog expansion, i.e., $f = g + \tau g_1 + \cdots$, we can employ τg_1 as f^1. Of course, under the smooth reconstruction at cell interfaces, e.g. Reconstruction-I, the explicit construction of τg_1 or fictitious f^1 is meaningless, since we KNOW the result of the integration of τg_1 or f^1 with respect to $\boldsymbol{\xi}$. The explicit functional form of τg_1 or f^1 becomes necessary in the case of discontinuous reconstruction of the diffusive terms. Finally, we mention that the present NS solver becomes first order accurate in time when it solves the structures of nonweak shock waves (cf. [7]). In this case, however, the employment of the NS equations is not appropriate and the Boltzmann equation should be used.

4.2. Polyatomic gases

The extension to the case of polyatomic gases can readily be done by assuming the equi-partition of the internal energy into each degree of freedom. Let us consider the case for an ideal gas with K internal degrees of freedom. We summarize the gadgets necessary for this extension below:

(i) The distribution function f has K additional arguments $\eta_1, \eta_2, \ldots, \eta_K$, which are the parameters of the internal degrees of freedom, i.e., $f(x_1, t, \boldsymbol{\xi}, \boldsymbol{\eta})$.

(ii) The macroscopic variables $\boldsymbol{h}$ are defined by

$$\boldsymbol{h} = \int\int \boldsymbol{\psi} f \, \mathrm{d}\boldsymbol{\xi} \, \mathrm{d}\boldsymbol{\eta}, \tag{37}$$

where $\boldsymbol{\psi} = (1, \xi_i, (\xi_k^2 + \eta_m^2)/2)^{\mathrm{T}}$ and the domain of the integration for $\boldsymbol{\xi}$ and that for $\boldsymbol{\eta}$ are R^3 and R^K, respectively.

(iii) The local Maxwellian g is given by

$$g = \frac{\rho}{(2\pi RT)^{(K+3)/2}} \exp\left[-\frac{(\xi_i - u_i)^2 + \eta_m^2}{2RT}\right], \tag{38}$$

and satisfies

$$\boldsymbol{h} = \int\int \boldsymbol{\psi} g \, \mathrm{d}\boldsymbol{\xi} \, \mathrm{d}\boldsymbol{\eta} \tag{39}$$

and

$$\boldsymbol{\Phi} = \int\int \xi_1 \boldsymbol{\psi} g \, \mathrm{d}\boldsymbol{\xi} \, \mathrm{d}\boldsymbol{\eta}. \tag{40}$$

4.3. Artificial equilibrium function

Up to now, we have regarded the equilibrium function as the local Maxwellian. If the local Maxwellian (9) [or (38)] is employed, the error functions appear in the formulas of the numerical fluxes. Since the computation of the error function is time consuming, simple equilibrium functions are preferable from the point of the computational efficiency. Perthame [9] employed a simple equilibrium function with bounded support. The multidimensional version of the equilibrium function of [9] is

$$g = \begin{cases} \frac{\rho}{[6RT]^{(3+K)/2}} & \text{for } (\boldsymbol{\xi}, \boldsymbol{\eta}) \in \Omega(u_i, T), \\ 0, & \text{other}, \end{cases} \tag{41}$$

where $\Omega(u_i,T)$ is the $3 + K$ dimensional cube defined by:

$$\Omega(u_i, T) = \left(\prod_{k=1}^{3} A_k\right) \times \left(\prod_{m=1}^{K} B_m\right), \tag{42}$$

$$A_k = \left[u_k - \sqrt{3RT} < \xi_k < u_k + \sqrt{3RT}\right], \tag{43}$$

$$B_m = \left[-\sqrt{3RT} < \eta_m < \sqrt{3RT}\right]. \tag{44}$$

It is easily verified that the above function satisfies the properties of the equilibrium function, Eqs. (39) and (40). This equilibrium function will be employed in Appendix A.

5. Numerical demonstration in 2D flow problems

In this section, we consider the case of a diatomic ideal gas ($\gamma = 1.4$) and carry out the numerical test of the kinetic scheme in the well-known problems of the double Mach reflection, forward-facing step, and shock boundary layer interaction. The first two problems are for the compressible Euler solver and the third one is for the compressible NS solver. The numerical scheme employed in these tests is 2D version of the hybrid kinetic scheme with the artificial equilibrium function of Eq. (41). The detailed construction of the scheme is explained in Appendix A. The explanation here employs the nondimensional variables and the notation is summarized in Appendix A (the reference values, ρ_*, T_*, etc., are taken from the upstream condition).

5.1. Boundary condition at a solid wall

Before going to the numerical computation, we mention the treatment of the boundary condition at a solid wall. The numerical flux there is computed from the canonical solution (13) [or Eq. (35)]. The values of $\tilde{\boldsymbol{h}}$ and their space derivatives at the boundary are prescribed or are computed from the data around the boundary by appropriate approximations. In all the numerical computations below, the flux at the solid wall is computed from the continuous approximation of the canonical solution.

5.2. Double Mach reflection of a Mach 10 shock from a wedge

This test case is a model problem of the reflection of a Mach 10 planar shock wave from a wedge. Initially, the shock makes a 60° angle with the wall located at $y = 0$ and $1/6 \leqslant x$ and hits the wall at $x = 1/6$.

For the details of the set up of the problem, we refer the reader to [13]. The uniform cell system with $\Delta x = \Delta y = 1/120$ is employed and $\Delta t/\Delta x$ is fixed to 0.012 during the computation. The hybridization parameter α is determined by Eq. (28) with $h_k = p$ and $C = 200$. No artificial viscosity is employed. Figs. 2–5 show the snapshot of the flow field at $t = 0.24$. The complicated structures in the flow are well resolved. Incidentally, the unit of the time employed in [13] is $L/(\gamma RT_*)^{1/2}$ and it is $L/(2RT_*)^{1/2}$ in the present paper. Thus, $t = 0.24$ corresponds to $t \sim 0.2$ in [13]. The efficiency of the present scheme is checked by comparing the CPU time with that for the downloadable software VH-1 [12], which employs the Lagrangian remap version of the Piecewise Parabolic Method (PPM) developed in [2]. Since this software is based on the directional splitting algorithm, the kinetic scheme for this algorithm is employed in the comparison. The computational costs for these schemes are practically identical. Incidentally, we have carried out the computation of the kinetic scheme that employs the local Maxwellian as the equilibrium function. The results are practically the same as those shown in Figs. 2–5; the results for these different equilibrium functions are almost indistinguishable in the figures. This shows that the functional form of equilibrium function is not essential and we can cheat the real gas nature under the condition of the equivalent flux. As for the computational efficiency, the employment of the artificial equilibrium function reduces the CPU time by about 40%.

5.3. A Mach 3 wind tunnel with a forward-facing step

The second numerical test deals with a Mach 3 flow in a wind tunnel with a forward-facing step. The set up is explained elsewhere, e.g. in [13], and thus, the explanation is omitted here. The uniform cell system with $\Delta x = \Delta y = 1/160$ is employed and $\Delta t/\Delta x$ is fixed to 0.1 during the computation. The hybridization parameter α is determined by Eq. (28) with $h_k = p$ and $C = 500$. Neither special technique for the region around the corner nor artificial viscosity is employed. Figs. 6–9 show the snapshot of flow field at $t = 4.8$, which corresponds to $t \sim 4$ in [13]. The structures in the flow are well resolved. In particular, the oscillations of entropy contours are very small except around the region where the Kelvin–Helmholtz instability occurs, which is in contrast to the result of [12].

5.4. Shock boundary layer interaction

This test case deals with the interaction of an oblique shock with a laminar boundary-layer on a nonslip and adiabatic wall. The shock makes a 32.6° angle with the wall, which is located at $y = 0$ and $0 \leqslant x$, and hits the boundary layer on the wall at $x = 1$. The Mach number of the shock wave is equal to 2 and the Reynolds number based on the upstream flow condition and the unit length is 2.96×10^5. The viscosity is computed according to the Sutherland law and the Prandtl number is fixed to 0.714. Since this problem is not sensitive to the bulk viscosity, only the results for $\bar{\chi} = 0$ will be shown. The computational domain is

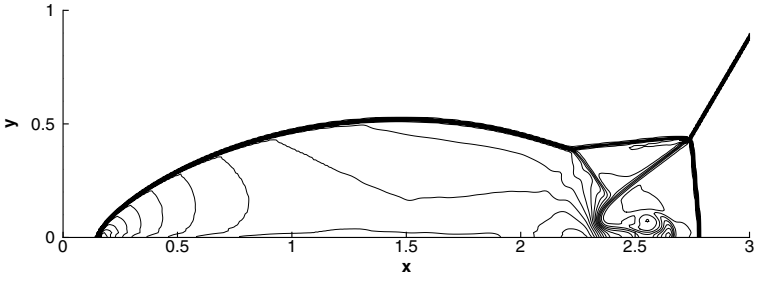

Fig. 2. Double Mach reflection. 30 Contours of the density ρ from 1.236 to 14.94.

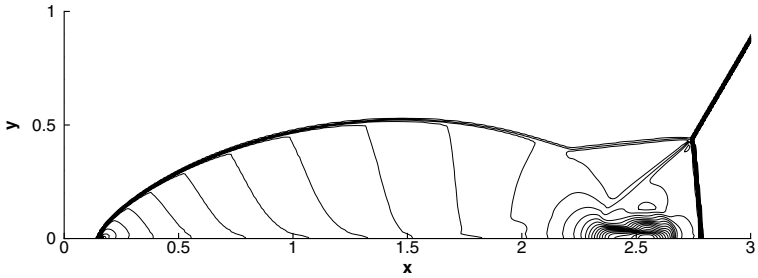

Fig. 3. Double Mach reflection. 30 Contours of the local Mach number $\sqrt{2(u^2+v^2)/\gamma T}$ from 0.11 to 3.36.

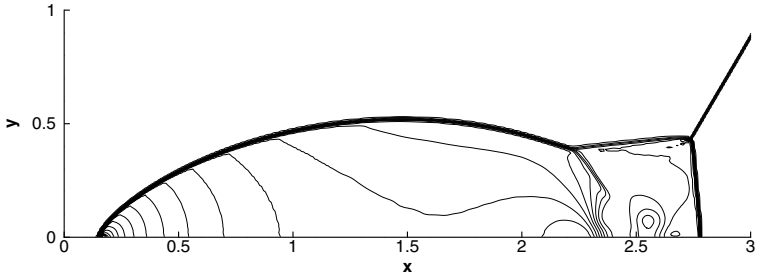

Fig. 4. Double Mach reflection. 30 Contours of the pressure p from 10.3 to 549.4.

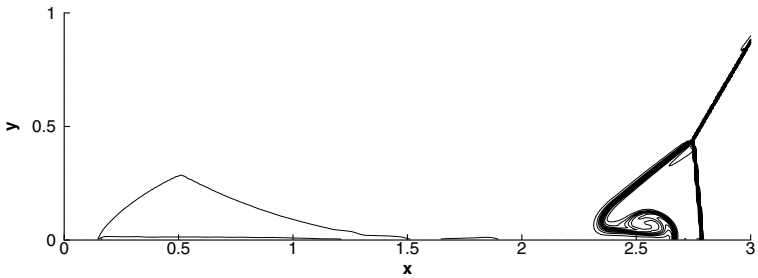

Fig. 5. Double Mach reflection. 30 Contours of p/ρ^{γ} from 1.318 to 19.48.

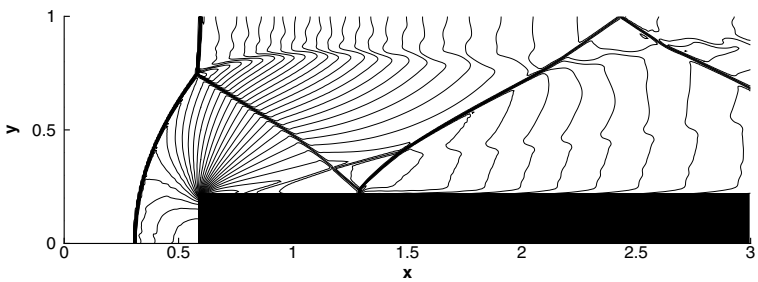

Fig. 6. Forward-facing step. 30 Contours of the density ρ from 0.183 to 4.334.

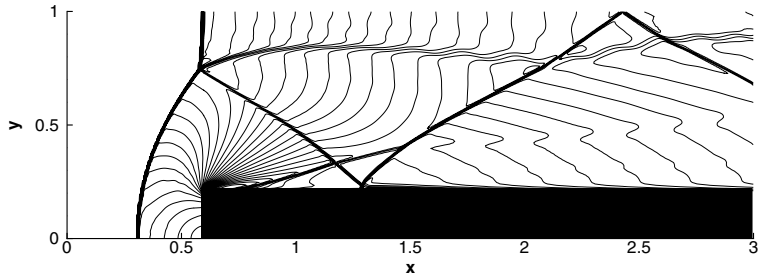

Fig. 7. Forward-facing step. 30 Contours of the local Mach number $\sqrt{2(u^2+v^2)/\gamma T}$ from 0.1 to 2.92.

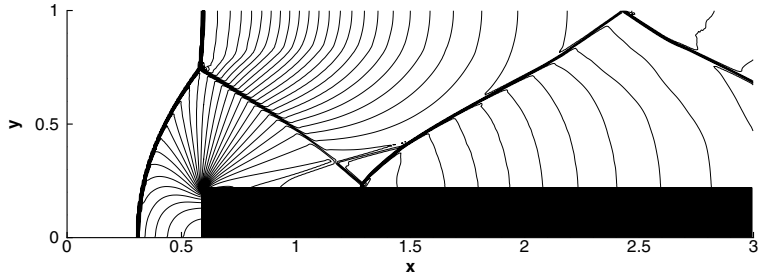

Fig. 8. Forward-facing step. 30 Contours of the pressure p from 0.275 to 11.82.

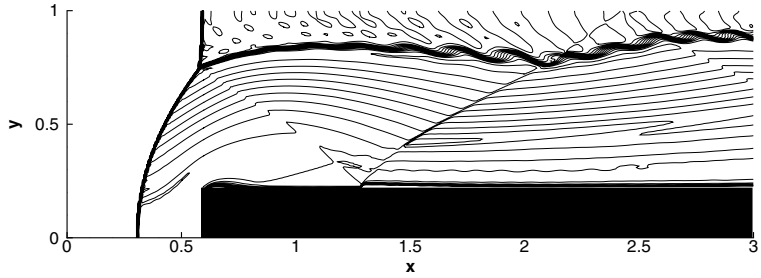

Fig. 9. Forward-facing step. 30 Contours of p/ρ^{γ} from 1.013 to 1.786.

the rectangle of $(-0.1 \leqslant x \leqslant 1.6) \times (0 \leqslant y \leqslant 1)$ and is divided into 120×100 nonuniform rectangular cells with the minimum width $\Delta x_{\min} = 5 \times 10^{-4}$ around $x = 0$ and the maximum width $\Delta x_{\max} = 1.5 \times 10^{-2}$ for x and the minimum width $\Delta y_{\min} = 5 \times 10^{-4}$ around $y = 0$ and the maximum width $\Delta y_{\max} = 1.25 \times 10^{-2}$ for y. The time step Δt is determined by $\Delta t/\Delta y_{\min} = 0.4$. The results of this steady boundary-value problem are obtained after the pursuit of long time evolution from an appropriate initial condition. The value of the hybridization parameter α is determined by Eq. (28) with $h_k = p$ and $C = 10$. Fig. 10 shows the pressure field. Since the width of the cell is much larger than the shock thickness, the accurate shock structure is not expected in the present computation. However, the present computation is carried out under the sufficient resolution to capture the boundary-layer. The results of the hybrid kinetic scheme and those of the preliminary kinetic scheme based on Reconstruction-II are compared in Figs. 11 and 12. While the difference between the result of 120×100 cell system and that of 240×200 cell system is small in the case of the hybrid scheme, the difference is quite large in the case of the preliminary scheme. The skin friction and

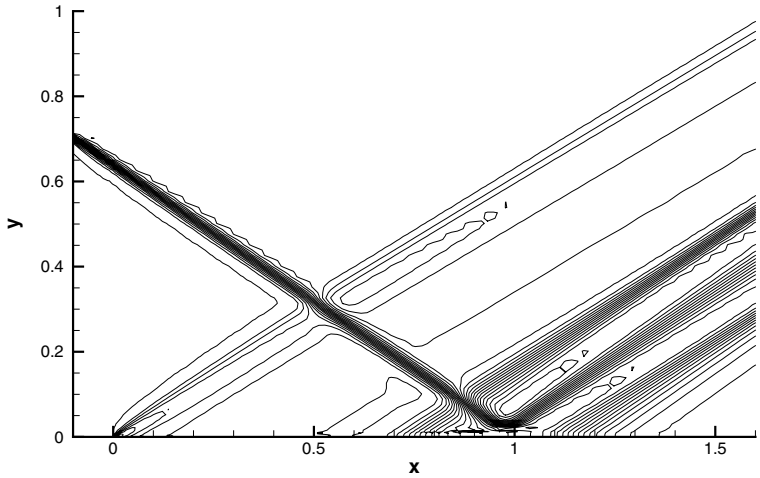

Fig. 10. Shock boundary layer interaction (120×100 cells). 30 Contours of p from 1 to 1.397.

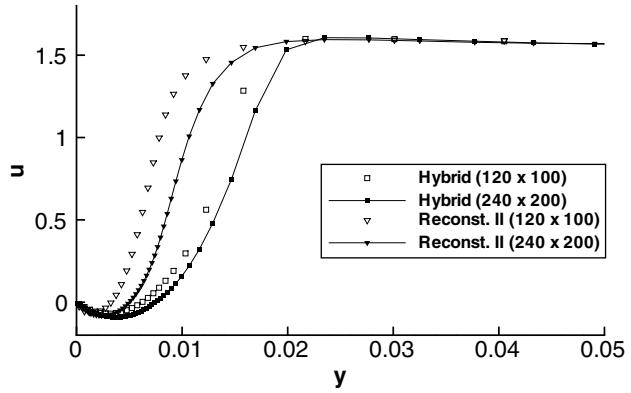

Fig. 11. Shock boundary layer interaction. Comparison of u distribution along $x = 1$.

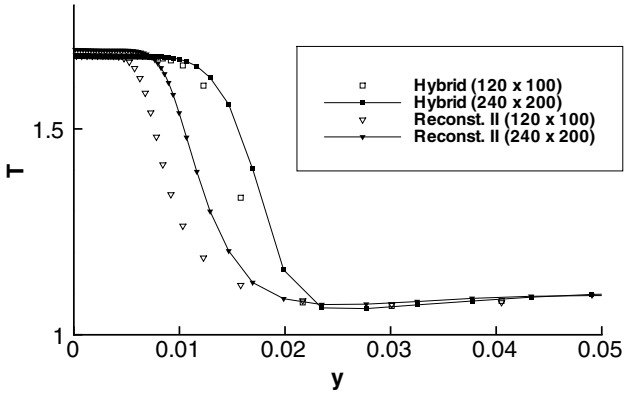

Fig. 12. Shock boundary layer interaction. Comparison of T distribution along $x = 1$.

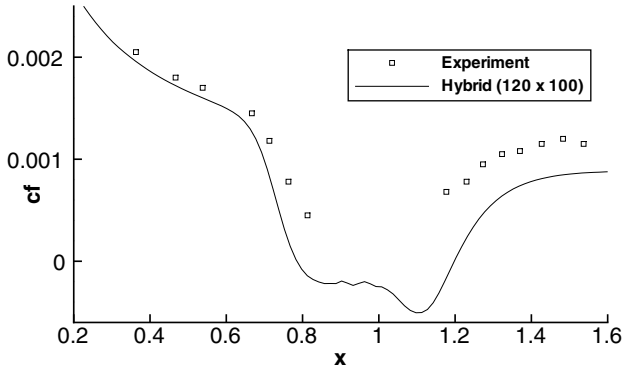

Fig. 13. Shock boundary layer interaction. Distribution of skin friction coefficient at the plate surface.

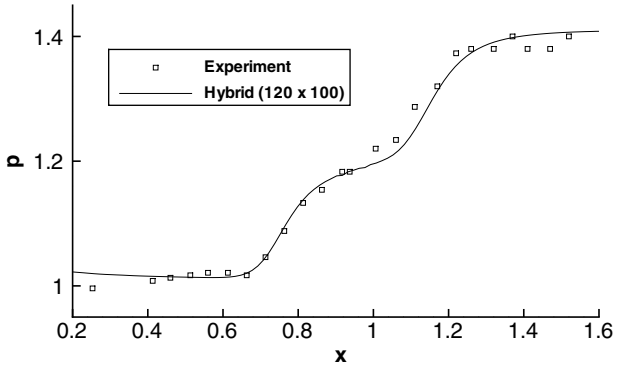

Fig. 14. Shock boundary layer interaction. Distribution of p at the plate surface.

pressure distributions at the plate surface are shown in Figs. 13 and 14, where the fair agreement with the experimental data [4] is confirmed. Incidentally, we have carried out the computation of the kinetic scheme that employs the local Maxwellian as the equilibrium function. The results are practically the same as those shown in Figs. 10–14; the results for the different equilibrium functions are almost indistinguishable in the figures. This shows that the equivalence in the flux is essential even in the case of the NS equations. As for the computational efficiency, the employment of the artificial equilibrium function reduces the CPU time by about 40% as in the case of the Euler equations.

6. Concluding remarks

The efficiency of a numerical method is judged by the cost required for obtaining solutions of the same quality and the cost is usually estimated by the CPU time, which is indeed one of the important factors determining development speed. We should, however, recall the fact that the cost consists of various factors. In fact, the electric cost required in the computation itself is much less than the salaries paid to the operating engineers. CFD is now used as a powerful tool of development researches in various fields of industry and the influence of cost of CFD education on society will be rapidly increasing unless the majority of the users are satisfied with the "black box". In the present study, we proposed simple derivation of

high-resolution schemes for the compressible Euler and Navier–Stokes equations aiming to reduce the cost of CFD education. Neither new theory nor new technique is devised in the present paper. Instead, the railroad method (or the Cauchy–Kowalevskaya procedure), van Leer's MUSCL reconstruction, Xu's hybrid reconstruction, and Perthame's artificial equilibrium function are integrated as one of the easiest-to-understand high-resolution schemes for compressible flows. Needless to say, the kinetic scheme is based on kinetic theory. As we have seen, however, any special techniques in kinetic theory, such as the asymptotic analysis of the Boltzmann equation, which requires cumbersome calculations, are not necessary as far as the gas-dynamic equations up to the level of the Navier–Stokes equations are concerned. Of course, the kinetic scheme is an appropriate topic as the introduction to kinetic theory for the students who have just completed the elementary course of gas-dynamics.

Appendix A. Kinetic scheme for 2D compressible flows

In this appendix, we consider the 2D compressible Navier–Stokes equations for ideal gases and give the explicit formulas of the numerical flux.

A.1. Basic equation and notation

The notation that will be employed in the appendix is independent of the text (except Section 5) and is summarized as follows. The ρ_* and T_* are the density and temperature of the gas at the reference state; $p_* = R\rho_* T_*$ (R is the specific gas constant per unit mass); L is the reference length; $t_* = L(2RT_*)^{-1/2}$ is the reference time; Lx_i is the Cartesian coordinates; $t_* t$ is the time; $(2RT_*)^{1/2}\xi_i$ is the translational velocity of the gas molecule; $(2RT_*)^{1/2}\eta_m$ ($m = 1,2,\ldots,K$) are the parameters of K internal degrees of freedom ($K = 0$ for monatomic gases and $K = 2$ for diatomic gases); $\rho_*(2RT_*)^{(3+K)/2}\mathrm{f}(x_i,t,\zeta_i,\eta_m)$ is the distribution function of the gas molecules; $\rho_*\rho$, $(2RT_*)^{1/2}u_i$, T_*T, p_*p ($p = \rho T$), p_*P_{ij}, and $p_*(2RT_*)^{1/2}Q_i$ are the density, flow velocity, temperature, pressure, stress tensor, and heat flow vector of the gas, respectively; $\gamma = C_p/C_v = 1 + R/C_v$ and $C_v = (3 + K)R/2$; μ_* is the viscosity at the reference state, $\mu_*\bar{\mu}$ is the viscosity, and $\mu_*\bar{\chi}$ is the bulk viscosity; $Re = \rho_* U_* L\mu_*^{-1}$ is the Reynolds number, where U_* is the reference speed of the flow (note that the flow velocity and the molecular velocity are not nondimensionalized by U_*), $Ma = U_*(\gamma RT_*)^{-1/2}$ is the Mach number, $Pr = C_p\mu_*\bar{\mu}\kappa^{-1}$ is the Prandtl number, where κ is the thermal conductivity of the gas.

The nondimensional compressible Navier–Stokes equations for ideal gases are written as:

$$\frac{\partial}{\partial t}\begin{pmatrix}\rho\\ \rho u_i\\ \rho[u_k^2 + T/(\gamma-1)]\end{pmatrix} + \frac{\partial}{\partial x_j}\begin{pmatrix}\rho u_j\\ \rho u_i u_j + P_{ij}/2\\ \rho u_j[u_k^2 + T/(\gamma-1)] + P_{kj}u_k + Q_j\end{pmatrix} = 0, \tag{A.1}$$

$$P_{ij} = p\delta_{ij} - \frac{(2\gamma)^{1/2}Ma}{Re}\left[\bar{\mu}\left(\frac{\partial u_i}{\partial x_j} + \frac{\partial u_j}{\partial x_i} - \frac{2}{3}\frac{\partial u_k}{\partial x_k}\delta_{ij}\right) + \bar{\chi}\frac{\partial u_k}{\partial x_k}\delta_{ij}\right], \tag{A.2}$$

$$Q_j = -\frac{\gamma}{\gamma-1}\frac{(\gamma/2)^{1/2}Ma}{PrRe}\bar{\mu}\frac{\partial T}{\partial x_j}. \tag{A.3}$$

From now on, we consider the case where the physical quantities are independent of x_3 and $u_3 = 0$. We will use x, y, u, and v instead of x_1, x_2, u_1, and u_2, respectively, i.e., $x = x_1$, $y = x_2$, $u = u_1$, and $v = u_2$. Then, the NS equations are rewritten as

$$\frac{\partial \boldsymbol{h}}{\partial t} + \frac{\partial \boldsymbol{\Phi}^{\mathrm{NS}}}{\partial x} + \frac{\partial \boldsymbol{\Psi}^{\mathrm{NS}}}{\partial y} = 0, \tag{A.4}$$

where:

$$\boldsymbol{h} = (\rho, \rho u, \rho v, \rho[u^2 + v^2 + T/(\gamma - 1)])^{\mathrm{T}}, \tag{A.5}$$

$$\boldsymbol{\Phi}^{\mathrm{NS}} = \boldsymbol{\Phi} + \boldsymbol{\Phi}^1, \quad \boldsymbol{\Psi}^{\mathrm{NS}} = \boldsymbol{\Psi} + \boldsymbol{\Psi}^1, \tag{A.6}$$

$$\boldsymbol{\Phi} = (\rho u, \rho u^2 + p/2, \rho uv, \rho u[u^2 + v^2 + T/(\gamma - 1)] + pu)^{\mathrm{T}}, \tag{A.7}$$

$$\boldsymbol{\Psi} = (\rho v, \rho uv, \rho v^2 + p/2, \rho v[u^2 + v^2 + T/(\gamma - 1)] + pv)^{\mathrm{T}}, \tag{A.8}$$

$$\boldsymbol{\Phi}^1 = (0, P_{11}/2, P_{21}/2, P_{11}u + P_{21}v + Q_1)^{\mathrm{T}}, \tag{A.9}$$

$$\boldsymbol{\Psi}^1 = (0, P_{12}/2, P_{22}/2, P_{12}u + P_{22}v + Q_2)^{\mathrm{T}}, \tag{A.10}$$

$$P_{11} = -\frac{\sqrt{2\gamma}Ma}{Re}\left[\bar{\mu}\left(\frac{4}{3}\frac{\partial u}{\partial x} - \frac{2}{3}\frac{\partial v}{\partial y}\right) + \bar{\chi}\left(\frac{\partial u}{\partial x} + \frac{\partial v}{\partial y}\right)\right], \tag{A.11}$$

$$P_{12} = P_{21} = -\frac{\sqrt{2\gamma}Ma}{Re}\bar{\mu}\left(\frac{\partial u}{\partial y} + \frac{\partial v}{\partial x}\right), \tag{A.12}$$

$$P_{22} = -\frac{\sqrt{2\gamma}Ma}{Re}\left[\bar{\mu}\left(-\frac{2}{3}\frac{\partial u}{\partial x} + \frac{4}{3}\frac{\partial v}{\partial y}\right) + \bar{\chi}\left(\frac{\partial u}{\partial x} + \frac{\partial v}{\partial y}\right)\right], \tag{A.13}$$

$$(Q_1, Q_2) = -\frac{\gamma^{3/2}\bar{\mu}Ma}{\sqrt{2}(\gamma - 1)RePr}\left(\frac{\partial T}{\partial x}, \frac{\partial T}{\partial y}\right). \tag{A.14}$$

The bulk viscosity is zero for monatomic gases ($\bar{\chi} = 0$ for $K = 0$) but it is generally not for polyatomic gases.

A.2. Finite volume method

We employ rectangular cells in xy plane. Let the cell (i,j) be the rectangle $[x^{i-1/2} < x < x^{i+1/2}] \times [y^{j-1/2} < y < y^{j+1/2}]$ and let $\boldsymbol{h}^{ij}(t)$ be the average of $\boldsymbol{h}(x,y,t)$ over the cell (i,j), which represents the value of $\boldsymbol{h}$ at the center of gravity of the cell (x^i,y^j). Then, the integral form of Eq. (A.4) is given by

$$\boldsymbol{h}^{ij}(\Delta t) = \boldsymbol{h}^{ij}(0) - \frac{1}{\Delta x}(\overline{\boldsymbol{F}}^{i+1/2,j} - \overline{\boldsymbol{F}}^{i-1/2,j}) - \frac{1}{\Delta y}(\overline{\boldsymbol{G}}^{i,j+1/2} - \overline{\boldsymbol{G}}^{i,j-1/2}), \tag{A.15}$$

where:

$$\overline{\boldsymbol{F}}^{i+1/2,j} = \int_0^{\Delta t} (\boldsymbol{\Phi} + \boldsymbol{\Phi}^1)(x^{i+1/2}, y^j, t)\, \mathrm{d}t, \tag{A.16}$$

$$\overline{\boldsymbol{G}}^{i,j+1/2} = \int_0^{\Delta t} (\boldsymbol{\Psi} + \boldsymbol{\Psi}^1)(x^i, y^{j+1/2}, t)\, \mathrm{d}t, \tag{A.17}$$

$\Delta x = x^{i+1/2} - x^{i-1/2}$ and $\Delta y = y^{j+1/2} - y^{j-1/2}$. As mentioned in Section 4.1, high order accuracy is not spoiled even when the first order accurate integration formula is applied to $\boldsymbol{\Phi}^1$ and $\boldsymbol{\Psi}^1$, i.e.:

$$\overline{\boldsymbol{F}}^{i+1/2,j} = \boldsymbol{F}^{i+1/2,j} + \Delta t \boldsymbol{\Phi}^1(x^{i+1/2}, y^j, 0), \tag{A.18}$$

$$\overline{\boldsymbol{G}}^{i,j+1/2} = \boldsymbol{G}^{i,j+1/2} + \Delta t \boldsymbol{\Psi}^1(x^i, y^{j+1/2}, 0), \tag{A.19}$$

$$\boldsymbol{F}^{i+1/2,j} = \int_0^{\Delta t} \boldsymbol{\Phi}(x^{i+1/2}, y^j, t)\, \mathrm{d}t, \tag{A.20}$$

$$\boldsymbol{G}^{i,j+1/2} = \int_0^{\Delta t} \boldsymbol{\Psi}(x^i, y^{j+1/2}, t)\, \mathrm{d}t, \tag{A.21}$$

which is easily seen from that fact $\mathbf{\Phi}^1$ and $\mathbf{\Psi}^1$ are proportional to the ratio $Ma/Re \sim Kn$ (Kn: the Knudsen number) and the time step Δt satisfies $Kn \lesssim \Delta t$ under the usual gas-dynamic computation. As stated in Section 4.1, the approximation of f^1 by Reconstruction-I is equivalent to the central finite difference approximation of $\mathbf{\Phi}^1$ and $\mathbf{\Psi}^1$. Thus, in the following section, we will consider only the numerical fluxes for the Euler equations.

A.3. 2D canonical solution for the Euler equations

The nondimensional conservative variables $\boldsymbol{h} = (\rho, \rho u, \rho v, (3+K)\rho T/2 + \rho[u^2+v^2])^{\mathrm{T}}$ are defined by the moments of f

$$\boldsymbol{h} = \int\int \boldsymbol{\psi} f \, \mathrm{d}\boldsymbol{\xi} \, \mathrm{d}\boldsymbol{\eta}, \tag{A.22}$$

where $\boldsymbol{\psi} = (1, \xi_1, \xi_2, \xi_1^2 + \xi_2^2 + \xi_3^2 + \eta_1^2 + \cdots + \eta_K^2)^{\mathrm{T}}$ and the domain of the integration with respect to $\boldsymbol{\xi}$ and that with respect to $\boldsymbol{\eta}$ are R^3 and R^K, respectively. In order to compute the numerical flux for the compressible Euler equations, the equilibrium function $g(h, \boldsymbol{\xi}, \boldsymbol{\eta})$ is introduced. The equilibrium function g must satisfy the conditions:

$$\boldsymbol{h} = \int\int \boldsymbol{\psi} g \, \mathrm{d}\boldsymbol{\xi} \, \mathrm{d}\boldsymbol{\eta}, \tag{A.23}$$

$$\mathbf{\Phi} = \int\int \xi_1 \boldsymbol{\psi} g \, \mathrm{d}\boldsymbol{\xi} \, \mathrm{d}\boldsymbol{\eta}, \quad \mathbf{\Psi} = \int\int \xi_2 \boldsymbol{\psi} g \, \mathrm{d}\boldsymbol{\xi} \, \mathrm{d}\boldsymbol{\eta}. \tag{A.24}$$

The nondimensional local Maxwellian

$$g = \frac{\rho}{(\pi T)^{(3+K)/2}} \exp\left[-\frac{(\xi_1 - u)^2 + (\xi_2 - v)^2 + \eta_m^2}{T} \right] \tag{A.25}$$

and the nondimensional version of the artificial equilibrium function in Section 4.3:

$$g = \begin{cases} \frac{\rho}{[6T]^{(3+K)/2}} & \text{for } (\boldsymbol{\xi}, \boldsymbol{\eta}) \in \Omega(u, v, T), \\ 0, & \text{other}, \end{cases} \tag{A.26}$$

$$\Omega(u, v, T) = \left(\prod_{i=1}^{3} A_i \right) \times \left(\prod_{m=1}^{K} B_m \right), \tag{A.27}$$

$$A_1 = \left[u - \sqrt{\frac{3T}{2}} < \xi_1 < u + \sqrt{\frac{3T}{2}} \right], \quad A_2 = \left[v - \sqrt{\frac{3T}{2}} < \xi_2 < v + \sqrt{\frac{3T}{2}} \right],$$

$$A_3 = \left[-\sqrt{\frac{3T}{2}} < \xi_3 < \sqrt{\frac{3T}{2}} \right], \quad B_m = \left[-\sqrt{\frac{3T}{2}} < \eta_m < \sqrt{\frac{3T}{2}} \right] \quad (m = 1, 2, \ldots, K), \tag{A.28}$$

satisfy the above conditions.

The numerical fluxes for the compressible Euler equations are computed from g whose macroscopic parameters $\boldsymbol{h}$ satisfy

$$\frac{\partial \boldsymbol{h}}{\partial t} + \frac{\partial \mathbf{\Phi}}{\partial x} + \frac{\partial \mathbf{\Psi}}{\partial y} = 0. \tag{A.29}$$

Then, the numerical fluxes $\boldsymbol{F}^{i+1/2,j}$ and $\boldsymbol{G}^{i,j+1/2}$ are formally written as:

$$\boldsymbol{F}^{i+1/2,j} = \int_0^{\Delta t} \int\int \xi_1 \boldsymbol{\psi} f_c(x^{i+1/2}, y^j, t, \boldsymbol{\xi}, \boldsymbol{\eta})\, \mathrm{d}\boldsymbol{\xi}\, \mathrm{d}\boldsymbol{\eta}\, \mathrm{d}t, \tag{A.30}$$

$$\boldsymbol{G}^{i,j+1/2} = \int_0^{\Delta t} \int\int \xi_2 \boldsymbol{\psi} f_c(x^i, y^{j+1/2}, t, \boldsymbol{\xi}, \boldsymbol{\eta})\, \mathrm{d}\boldsymbol{\xi}\, \mathrm{d}\boldsymbol{\eta}\, \mathrm{d}t, \tag{A.31}$$

where f_c is the 2D canonical solution defined by:

$$f_c = g - t\frac{\partial g}{\partial h_k}(\Delta\Phi_k + \Delta\Psi_k), \tag{A.32}$$

$$\Delta\Phi_k = \int\int \xi_1 \psi_k \frac{\partial g}{\partial \tilde{h}_m}\frac{\partial \tilde{h}_m}{\partial x}\, \mathrm{d}\boldsymbol{\xi}\, \mathrm{d}\boldsymbol{\eta}, \tag{A.33}$$

$$\Delta\Psi_k = \int\int \xi_2 \psi_k \frac{\partial g}{\partial \tilde{h}_m}\frac{\partial \tilde{h}_m}{\partial y}\, \mathrm{d}\boldsymbol{\xi}\, \mathrm{d}\boldsymbol{\eta}. \tag{A.34}$$

Each term of the canonical solution is evaluated at $(x,y,t) = (x^{i+1/2},y^j,0)$ for $\boldsymbol{F}^{i+1/2,j}$ and $(x,y,t) = (x^i,y^{j+1/2},0)$ for $\boldsymbol{G}^{i,j+1/2}$.

A.4. Data construction

We summarize the construction of the necessary data for the computation of the numerical flux. Here, for simplicity, we consider the case of uniform cell systems. The extension to nonuniform case can be done by minor modification, and thus, it is omitted here.

From the data of the conservative variables $\boldsymbol{h}^{ij}$, the corresponding values of the primitive variable $\tilde{\boldsymbol{h}}={}^t(\rho,u,v,T)$, i.e., $\tilde{\boldsymbol{h}}^{ij}$, are immediately obtained. The numerical fluxes $\boldsymbol{F}^{i+1/2,j}$ and $\boldsymbol{\Phi}^1$ are computed from the values of the primitive variables and their spatial derivatives at $(x,y) = (x^{i+1/2},y^j)$. The values of $\tilde{\boldsymbol{h}}$ and $\partial\tilde{\boldsymbol{h}}/\partial\beta$ $(\beta = x,y)$ employed in the computation of $\boldsymbol{\Phi}^1$ are obtained as follows. $\tilde{\boldsymbol{h}}$ and $\partial\tilde{\boldsymbol{h}}/\partial x$ are computed from the data $\tilde{\boldsymbol{h}}^{ij}$ and $\tilde{\boldsymbol{h}}^{i+1,j}$, and $\partial\tilde{\boldsymbol{h}}/\partial y$ is computed from the data $\tilde{\boldsymbol{h}}^{i+1/2,j-1}$ and $\tilde{\boldsymbol{h}}^{i+1/2,j+1}$ by means of the linear interpolation. The values employed in the computation of $\boldsymbol{F}^{i+1/2,j}$ are obtained as follows. $\tilde{\boldsymbol{h}}$ and $\partial\tilde{\boldsymbol{h}}/\partial\beta$ at $(x,y) = (x^{i+1/2}\pm 0,y^j)$, which will be denoted by $\tilde{\boldsymbol{h}}_{\pm}^{i+1/2,j}$ and $(\partial_\beta\tilde{\boldsymbol{h}})_{\pm}^{i+1/2,j}$, respectively, are computed by means of the van Leer limiter (the other limiters can be employed); $\tilde{\boldsymbol{h}}_{+}^{i+1/2,j}$ and $(\partial_x\tilde{\boldsymbol{h}})_{+}^{i+1/2,j}$ are computed from $\tilde{\boldsymbol{h}}^{i,j}$, $\tilde{\boldsymbol{h}}^{i+1,j}$ and $\tilde{\boldsymbol{h}}^{i+2,j}$, and $\tilde{\boldsymbol{h}}_{-}^{i+1/2,j}$ and $(\partial_x\tilde{\boldsymbol{h}})_{-}^{i+1/2,j}$ are done from $\tilde{\boldsymbol{h}}^{i-1,j}$, $\tilde{\boldsymbol{h}}^{ij}$ and $\tilde{\boldsymbol{h}}^{i+1,j}$; $(\partial_y\tilde{\boldsymbol{h}})_{\pm}^{i+1/2,j}$ is computed from $\tilde{\boldsymbol{h}}^{i+1/2\pm1/2,j-1}$, $\tilde{\boldsymbol{h}}^{i+1/2\pm1/2,j}$, and $\tilde{\boldsymbol{h}}^{i+1/2\pm1/2,j+1}$. The data necessary for the computation of $\boldsymbol{G}^{i,j+1/2}$ and $\boldsymbol{\Psi}^1$ are defined and are computed in the similar way (exchange the roles of x and y), and thus, the explanation is omitted.

A.5. Formulas for $\boldsymbol{F}^{i+1/2,j}$

We give the formulas for $\boldsymbol{F}^{i+1/2,j}$ below; the formulas for $\boldsymbol{G}^{i,j+1/2}$ are obtained by the simple modification of those for $\boldsymbol{F}^{i+1/2,j}$.

The hybrid version of the 2D canonical solution (A.32) is

$$f_c = \alpha g^{\mathrm{II}} + (1-\alpha)g^{\mathrm{III}} - t\left(\frac{\partial g}{\partial h_k}\right)^{\mathrm{III}}(\Delta\Phi_k^{\mathrm{II}} + \Delta\Psi_k^{\mathrm{II}}), \tag{A.35}$$

$$\Delta\Phi_k^{\mathrm{II}} = \int\int \xi_1 \psi_k \left(\frac{\partial g}{\partial \tilde{h}_m} \frac{\partial \tilde{h}_m}{\partial x} \right)^{\mathrm{II}} \mathrm{d}\boldsymbol{\xi}\, \mathrm{d}\boldsymbol{\eta}, \tag{A.36}$$

$$\Delta\Psi_k^{\mathrm{II}} = \int\int \xi_2 \psi_k \left(\frac{\partial g}{\partial \tilde{h}_m} \frac{\partial \tilde{h}_m}{\partial y} \right)^{\mathrm{II}} \mathrm{d}\boldsymbol{\xi}\, \mathrm{d}\boldsymbol{\eta}, \tag{A.37}$$

where each term is evaluated at $(x,y,t) = (x^{i+1/2}, y^j, 0)$. We introduce the functional defined by

$$\mathscr{F}[b] = \int\int \xi_1 \boldsymbol{\psi} b \, \mathrm{d}\boldsymbol{\xi}\, \mathrm{d}\boldsymbol{\eta}. \tag{A.38}$$

Then, $\boldsymbol{F}^{i+1/2,j}$ is given by

$$\boldsymbol{F}^{i+1/2,j} = \Delta t(\alpha \mathscr{F}[g^{\mathrm{II}}] + (1-\alpha)\mathscr{F}[g^{\mathrm{III}}]) - \frac{\Delta t^2}{2} \mathscr{F}\left[\left(\frac{\partial g}{\partial h_k} \right)^{\mathrm{III}} \right] (\Delta\Phi_k^{\mathrm{II}} + \Delta\Psi_k^{\mathrm{II}}). \tag{A.39}$$

We will show the explicit formulas of the functionals in Eq. (A.39) for the case of the artificial equilibrium function, Eq. (A.26), with $K = 2$, i.e., $\boldsymbol{h} = {}^t(\rho, \rho u, \rho v, \rho(u^2 + v^2 + 5T/2))$. For the concise expression of the formulas, we introduce the following functions and abbreviation:

$$\Theta(s) = \frac{|s| + s}{2}, \quad \Lambda(s) = \frac{s - |s|}{2}. \tag{A.40}$$

$$S(s) = \begin{cases} 1 & s > 0 \\ 0 & s \leqslant 0 \end{cases}, \quad W(s) = \begin{cases} 1 & s < 0 \\ 0 & s \geqslant 0 \end{cases}, \tag{A.41}$$

$$\tilde{\boldsymbol{h}}_\pm = \tilde{\boldsymbol{h}}_\pm^{i+1/2,j}, \quad \partial_\beta \tilde{\boldsymbol{h}}_\pm = (\partial \tilde{\boldsymbol{h}}/\partial\beta)_\pm^{i+1/2,j}, \tag{A.42}$$

$$a_\pm = \Theta(u_- \pm \sqrt{3T_-/2}), \quad b_\pm = \Lambda(u_+ \pm \sqrt{3T_+/2}), \tag{A.43}$$

$$c_\pm = \frac{\rho_\pm}{\sqrt{6T_\pm}}, \quad d_\pm = \frac{1}{\sqrt{6T_\pm}}, \quad e_\pm = \frac{1}{4T_\pm}, \quad m_\pm = T_\pm + \frac{v_\pm^2}{2}, \tag{A.44}$$

$$q_\pm = v_\pm^2 + \frac{T_\pm}{2}, \quad r_\pm = v_\pm^3 + 3v_\pm T_\pm, \tag{A.45}$$

$$\begin{aligned} \zeta_\pm &= S(u_- + \sqrt{3T_-/2}) \pm S(u_- - \sqrt{3T_-/2}), \\ \omega_\pm &= W(u_+ + \sqrt{3T_+/2}) \pm W(u_+ - \sqrt{3T_+/2}), \end{aligned} \tag{A.46}$$

$$A_\pm^n = (a_+)^n \pm (a_-)^n, \quad B_\pm^n = (b_+)^n \pm (b_-)^n. \tag{A.47}$$

Then, $\boldsymbol{h}^{\mathrm{III}}$ are given by:

$$h_1^{\mathrm{III}} = c_- A_-^1 + c_+ B_-^1, \tag{A.48}$$

$$h_2^{\mathrm{III}} = \frac{1}{2}[c_- A_-^2 + c_+ B_-^2], \tag{A.49}$$

$$h_3^{\mathrm{III}} = c_- v_- A_-^1 + c_+ v_+ B_-^1, \tag{A.50}$$

$$h_4^{\mathrm{III}} = c_-(A_-^3/3 + 2m_- A_-^1) + c_+(B_-^3/3 + 2m_+ B_-^1), \tag{A.51}$$

and ρ^{III}, u^{III}, v^{III}, and T^{III} are immediately computed from the values of h_k^{III} $(k = 1, 2, 3, 4)$. Hereafter, we will omit the superscript III from $\boldsymbol{h}^{\mathrm{III}}$, i.e., $\rho^{\mathrm{III}} \to \rho$, $u^{\mathrm{III}} \to u$, and so on. Then, $\mathscr{F}[g^{\mathrm{III}}]$ is given by

$$\mathscr{F}[g^{\mathrm{III}}] = \begin{pmatrix} \rho u \\ \rho[u^2 + T/2] \\ \rho u v \\ \rho u[u^2 + v^2 + 7T/2] \end{pmatrix} \tag{A.52}$$

and $\mathscr{F}[(\partial g/\partial h_k)^{\mathrm{III}}]$ is given by

$$\mathscr{F}_i\left[\left(\frac{\partial g}{\partial h_k}\right)^{\mathrm{III}}\right] = \mathscr{R}_{ij}\mathscr{H}_{jk}, \tag{A.53}$$

where:

$$\mathscr{R}_{ij} = \frac{\partial}{\partial \tilde{h}_j}\int \xi_1 \psi_i g \,\mathrm{d}\boldsymbol{\xi}\,\mathrm{d}\boldsymbol{\eta}, \tag{A.54}$$

$$\mathscr{H}_{jk} = \frac{\partial \tilde{h}_j}{\partial h_k} \tag{A.55}$$

and the matrix representation of $\mathscr{R}_{ij}$ and $\mathscr{H}_{jk}$ is:

$$\mathscr{R} = \begin{pmatrix} u & \rho & 0 & 0 \\ u^2 + \frac{T}{2} & 2\rho u & 0 & \frac{\rho}{2} \\ uv & \rho v & \rho u & 0 \\ u\left(u^2 + v^2 + \frac{7T}{2}\right) & \rho\left(3u^2 + v^2 + \frac{7T}{2}\right) & 2\rho uv & \frac{7\rho u}{2} \end{pmatrix}, \tag{A.56}$$

$$\mathscr{H} = \begin{pmatrix} 1 & 0 & 0 & 0 \\ -\frac{u}{\rho} & \frac{1}{\rho} & 0 & 0 \\ -\frac{v}{\rho} & 0 & \frac{1}{\rho} & 0 \\ \frac{-5T+2(u^2+v^2)}{5\rho} & -\frac{4u}{5\rho} & -\frac{4v}{5\rho} & \frac{2}{5\rho} \end{pmatrix}. \tag{A.57}$$

The numerical flux $\mathscr{F}[g^{\mathrm{II}}]$ is given by:

$$\mathscr{F}_1[g^{\mathrm{II}}] = (c_-/2)A_-^2 + (c_+/2)B_-^2, \tag{A.58}$$

$$\mathscr{F}_2[g^{\mathrm{II}}] = (c_-/3)A_-^3 + (c_+/3)B_-^3, \tag{A.59}$$

$$\mathscr{F}_3[g^{\mathrm{II}}] = (c_- v_-/2)A_-^2 + (c_+ v_+/2)B_-^2, \tag{A.60}$$

$$\mathscr{F}_4[g^{\mathrm{II}}] = c_-(A_-^4/4 + m_- A_-^2) + c_+(B_-^4/4 + m_+ B_-^2). \tag{A.61}$$

$\Delta\boldsymbol{\Phi}^{\mathrm{II}}$ and $\Delta\boldsymbol{\Psi}^{\mathrm{II}}$ are given by:

$$\Delta\boldsymbol{\Phi}^{\mathrm{II}} = \mathscr{R}^+\partial_x\tilde{\boldsymbol{h}}_- + \mathscr{R}^-\partial_x\tilde{\boldsymbol{h}}_+, \tag{A.62}$$

$$\Delta\boldsymbol{\Psi}^{\mathrm{II}} = \mathscr{B}^+\partial_y\tilde{\boldsymbol{h}}_- + \mathscr{B}^-\partial_y\tilde{\boldsymbol{h}}_+, \tag{A.63}$$

where:

$$\mathscr{R}_{ij}^{\pm} = \frac{\partial}{\partial \tilde{h}_j}\int\int_{\xi_1 \gtrless 0} \psi_i \xi_1 g \,\mathrm{d}\boldsymbol{\xi}\,\mathrm{d}\boldsymbol{\eta}, \tag{A.64}$$

$$\mathscr{B}_{ij}^{\pm} = \frac{\partial}{\partial \tilde{h}_j}\int\int_{\xi_1 \gtrless 0} \psi_i \xi_2 g \,\mathrm{d}\boldsymbol{\xi}\,\mathrm{d}\boldsymbol{\eta}, \tag{A.65}$$

$$\mathscr{R}^+_{11} = \frac{d_- A^2_-}{2}, \quad \mathscr{R}^+_{12} = c_- A^1_-, \quad \mathscr{R}^+_{13} = 0, \quad \mathscr{R}^+_{14} = e_-(\rho_- A^1_+ - c_- A^2_-), \quad \mathscr{R}^+_{21} = \frac{d_- A^3_-}{3},$$

$$\mathscr{R}^+_{22} = c_- A^2_-, \quad \mathscr{R}^+_{23} = 0, \quad \mathscr{R}^+_{24} = \rho_- e_- A^2_+ - \frac{c_- A^3_-}{6T_-}, \quad \mathscr{R}^+_{31} = \frac{v_- d_- A^2_-}{2}, \quad \mathscr{R}^+_{32} = v_- \mathscr{R}^+_{12},$$

$$\mathscr{R}^+_{33} = \frac{\mathscr{R}^+_{22}}{2}, \quad \mathscr{R}^+_{34} = v_- \mathscr{R}^+_{14}, \quad \mathscr{R}^+_{41} = d_-\left(\frac{A^4_-}{4} + m_- A^2_-\right), \quad \mathscr{R}^+_{42} = c_-(A^3_- + 2m_- A^1_-),$$

$$\mathscr{R}^+_{43} = v_- \mathscr{R}^+_{22}, \quad \mathscr{R}^+_{44} = -\frac{c_- e_- A^4}{2} + \rho_- e_- A^3_+ + c_- e_-(2T_- - v^2_-)A^2_- + \frac{\rho_- m_- A^1_+}{2T_-}, \tag{A.66}$$

$$\mathscr{R}^-_{11} = \frac{d_+ B^2_-}{2}, \quad \mathscr{R}^-_{12} = c_+ B^1_-, \quad \mathscr{R}^-_{13} = 0, \quad \mathscr{R}^-_{14} = e_+(\rho_+ B^1_+ - c_+ B^2_-), \quad \mathscr{R}^-_{21} = \frac{d_+ B^3_-}{3},$$

$$\mathscr{R}^-_{22} = c_+ B^2_-, \quad \mathscr{R}^-_{23} = 0, \quad \mathscr{R}^-_{24} = \rho_+ e_+ B^2_+ - \frac{c_+ B^3_-}{6T_+}, \quad \mathscr{R}^-_{31} = \frac{v_+ d_+ B^2_-}{2}, \quad \mathscr{R}^-_{32} = v_+ \mathscr{R}^-_{12},$$

$$\mathscr{R}^-_{33} = \frac{\mathscr{R}^-_{22}}{2}, \quad \mathscr{R}^-_{34} = v_+ \mathscr{R}^-_{14}, \quad \mathscr{R}^-_{41} = d_+\left(\frac{B^4_-}{4} + m_+ B^2_-\right), \quad \mathscr{R}^-_{42} = c_+(B^3_- + 2m_+ B^1_-),$$

$$\mathscr{R}^-_{43} = v_+ \mathscr{R}^-_{22}, \quad \mathscr{R}^-_{44} = -\frac{c_+ e_+ B^4_-}{2} + \rho_+ e_+ B^3_+ + c_+ e_+(2T_+ - v^2_+)B^2_- + \frac{\rho_+ m_+ B^1_+}{2T_+}, \tag{A.67}$$

$$\mathscr{B}^+_{11} = d_- v_- A^1_-, \quad \mathscr{B}^+_{12} = c_- v_- \zeta_-, \quad \mathscr{B}^+_{13} = c_- A^1_-, \quad \mathscr{B}^+_{14} = e_- v_-(\rho_- \zeta_+ - 2c_- A^1_-),$$

$$\mathscr{B}^+_{21} = \frac{d_- v_- A^2_-}{2}, \quad \mathscr{B}^+_{22} = c_- v_- A^1_-, \quad \mathscr{B}^+_{23} = \frac{c_- A^2_-}{2}, \quad \mathscr{B}^+_{24} = v_- e_-(\rho_- A^1_+ - c_- A^2_-),$$

$$\mathscr{B}^+_{31} = d_- q_- A^1_-, \quad \mathscr{B}^+_{32} = c_- q_- \zeta_-, \quad \mathscr{B}^+_{33} = 2v_- c_- A^1_-, \quad \mathscr{B}^+_{34} = e_-[(T_- - 2v^2_-)c_- A^1_- + \rho_- q_- \zeta_+],$$

$$\mathscr{B}^+_{41} = d_-\left(r_- A^1_- + \frac{v_- A^3_-}{3}\right), \quad \mathscr{B}^+_{42} = c_-(r_- \zeta_- + v_- A^2_-), \quad \mathscr{B}^+_{43} = c_-\left[3(T_- + v^2_-)A^1_- + \frac{A^3_-}{3}\right],$$

$$\mathscr{B}^+_{44} = -\frac{v_- c_- A^3_-}{6T_-} + \rho_- v_- e_- A^2_+ + 2c_- v_- e_-(3T_- - v^2_-)A^1_- + e_- \rho_- r_- \zeta_+, \tag{A.68}$$

$$\mathscr{B}^-_{11} = d_+ v_+ B^1_-, \quad \mathscr{B}^-_{12} = c_+ v_+ \omega_-, \quad \mathscr{B}^-_{13} = c_+ B^1_-, \quad \mathscr{B}^-_{14} = e_+ v_+(\rho_+ \omega_+ - 2c_+ B^1_-),$$

$$\mathscr{B}^-_{21} = \frac{d_+ v_+ B^2_-}{2}, \quad \mathscr{B}^-_{22} = c_+ v_+ B^1_-, \quad \mathscr{B}^-_{23} = \frac{c_+ B^2_-}{2}, \quad \mathscr{B}^-_{24} = v_+ e_+(\rho_+ B^1_+ - c_+ B^2_-),$$

$$\mathscr{B}^-_{31} = d_+ q_+ B^1_-, \quad \mathscr{B}^-_{32} = c_+ q_+ \omega_-, \quad \mathscr{B}^-_{33} = 2v_+ c_+ B^1_-, \quad \mathscr{B}^-_{34} = e_+[(T_+ - 2v^2_+)c_+ B^1_- + \rho_+ q_+ \omega_+],$$

$$\mathscr{B}^-_{41} = d_+\left(r_+ B^1_- + \frac{v_+ B^3_-}{3}\right), \quad \mathscr{B}^-_{42} = c_+(r_+ \omega_- + v_+ B^2_-), \quad \mathscr{B}^-_{43} = c_+\left[3(T_+ + v^2_+)B^1_- + \frac{B^3_-}{3}\right],$$

$$\mathscr{B}^-_{44} = -\frac{v_+ c_+ B^3_-}{6T_+} + \rho_+ v_+ e_+ B^2_+ + 2c_+ v_+ e_+(3T_+ - v^2_+)B^1_- + e_+ \rho_+ r_+ \omega_+. \tag{A.69}$$

The formulas for $\boldsymbol{F}^{i+1/2,j}$ are now completed. The formulas for $\boldsymbol{G}^{i,j+1/2}$ can easily be obtained from the above formulas by the following manipulation: (i) exchange x and y; (ii) exchange u and v; (iii) exchange the second component of $\boldsymbol{F}^{i+1/2,j}$ (the momentum flux in the x-direction) and the third component (the momentum flux in the y-direction).

References

[1] S.Y. Chou, D. Baganoff, Kinetic flux-vector splitting for the Navier–Stokes equations, J. Comput. Phys. 130 (1997) 217–230.
[2] P. Colella, P. Woodward, The piecewise paraboric method (PPM) for gas-dynamic simulations, J. Comput. Phys. 54 (1984) 174–201.
[3] S.M. Deshpande, A second order accurate kinetic-theory based method for inviscid compressible flows, NASA Langley Tech. paper No. 2613, 1986.
[4] R.J. Hakkinen, L. Greber, L. Trilling, S.S. Abarbanel, NASA Memo. 2–18–59W, NASA, 1959.
[5] T. Ohwada, Boltzmann schemes for the compressible Navier–Stokes equations, in: T.J. Bartel, M. Gallis (Eds.), Rarefied Gas Dynamics, AIP Conference Proceedings, vol. 585, American Institute of Physics, 2001, pp. 321–328.
[6] T. Ohwada, On the construction of kinetic schemes, J. Comput. Phys. 177 (2002) 156–175.
[7] T. Ohwada, S. Kobayashi, Management of discontinuous reconstruction in kinetic schemes, J. Comput. Phys. 197 (2004) 116–138.
[8] T. Ohwada, K. Xu, The kinetic scheme for the full-Burnett equations, J. Comput. Phys. 201 (2004) 315–332.
[9] B. Perthame, Second-order Boltzmann schemes for the compressible Euler equations in one and two space dimensions, SIAM J. Numer. Anal. 29 (1992) 1–19.
[10] D.I. Pullin, Direct simulation methods for compressible inviscid ideal gas flow, J. Comput. Phys. 34 (1980) 231–244.
[11] E.F. Toro, Riemann Solvers and Numerical Methods for Fluid Dynamics: A Practical Introduction, second ed., Springer, Berlin, 1999.
[12] The Virginia Numerical Bull Session ideal hydrodynamics PPMLR, Version 1.0, 1991. Available from: <http://wonka.physics.ncsu.edu/pub/VH-1/index.html>.
[13] P. Woodward, P. Colella, The numerical simulation of two-dimensional fluid flow with strong shocks, J. Comput. Phys. 54 (1984) 115–173.
[14] K. Xu, Gas-kinetic scheme for unsteady compressible flow simulations, VKI for Fluid Dynamic Lecture Series 1998–03, 1998.
[15] K. Xu, A gas-kinetic BGK scheme for the Navier–Stokes equations and its connection with artificial dissipation and Godunov method, J. Comput. Phys. 171 (2001) 289–335.
[16] B. van Leer, Towards the ultimate conservative difference scheme IV, a new approach to numerical convection, J. Comput. Phys. 23 (1977) 276–299.